

University of Tartu
Institute of Computer Science
Computer Science curriculum

Kristiina Pokk

Exploring how images are represented in human brain activity

Bachelor's thesis (9 ECTS)

Supervisors: Dr. Raul Vicente
Dr. Jaan Aru

Tartu 2016

Exploring how images are represented in human brain activity

Abstract

This bachelor thesis explores how images are represented in human brain activity. Data used in this thesis were collected in the University Hospital of Lyon with experiments where human neural activity was recorded with intracranial electrodes during a simple visual task. The aim of this thesis is to analyse the data, more specifically the activity in the high-gamma frequency range, with unsupervised machine learning methods to find structure in it. In particular, similarity of neural responses (recorded by electrodes) to images and the differences in activity according to image categories.

Visualization and biclustering were used in this thesis. Out of the two analysis methods used, visualization was more successful. Among image categories used, images of faces stood out the best. The houses and scrambled images clustered to some extent as well. Visualizing electrodes resulted in pronounced clusters emerging, which were heterogeneous in their nature. Biclustering gave no noteworthy results.

Keywords: high-gamma frequency, unsupervised machine learning, visualization, biclustering

CERCS: P170

Piltide kujutamine inimese ajutegevuses

Lühikokkuvõte

Antud bakalaureusetöö uurib, kuidas on pildid kujutatud inimese ajutegevuses. Andmestik, mida töös kasutatakse, pärineb Lyoni Ülikooli haiglas tehtud uuringutest, kus mõõdeti intrakraniaalsete elektrootide abil inimese ajutegevust visuaalse ülesande ajal. Bakalaureusetöö eesmärk on analüüsida neid andmeid, täpsemalt kõrge gamma sageduse vahemikus olevat aktiivsust, juhendamata masinõppe meetoditega. Antud bakalaureusetöös kasutati erinevaid algoritme, et leida andmetest struktuuri, mis kirjeldaks elektrootide abil salvestatud visuaalse stiimuli ajal toimunud reaktsioonide sarnasusi. Lisaks analüüsiti kuivõrd on võimalik eristada pildi kategooriaid (majad, näod, loomad jne.) vastavalt tekkinud aju aktiivsusele.

Kasutatud analüüsi meetoditest oli edukaim visualiseerimine. Katses esitatud pildigruppidest eristusid kõige paremini nägude kujutised. Samuti klasterdusid mingil määral majad ja skrambleeritud (segipaisatud) pildid. Elektrootide visualiseerimisel tekkisid selged klastrid, mis koosnesid aga mitmest Brodmanni piirkonnast pärit andmepunktidest. Kahendklasterdamine tähelepanuväärseid tulemusi ei andnud

Võtmesõnad: kõrge gamma, juhendamata masinõppe, visualiseerimine, kahendklasterdamine

CERCS: P170

Contents

1	Introduction.....	5
2	Methods.....	7
2.1	Collecting data.....	7
2.2	Analysing methods.....	9
2.2.1	Visualization.....	9
2.2.2	Biclustering.....	10
3	Results.....	13
3.1	Structure across images.....	13
3.2	Structure of neural activity.....	16
3.3	Biclustering.....	19
4	Discussion.....	23
4.1	Interpretation of results.....	23
4.2	Limitations.....	24
4.3	Future work.....	24
5	Conclusion.....	25
6	References.....	26
7	Appendix.....	28
8	Licence.....	29

1 Introduction

Every time we open our eyes, our brain is presented with a complex visual field surrounding us. We as humans perceive depth, different colours and shapes. We not only see, what it is that is in front of us, but also recognize our environment, people and objects around us. This is not only true for stationary images. The brain is also adapted to deal with motion and the ever changing visual environment and therefore rapidly changing information. Even when we are the ones who create motion, move our eyes or head, the mind follows and the image moves in a smooth way that we think of as natural.

Vision is a predominant sense in humans' everyday lives. It constantly provides us with important data, helps to make sense of our surroundings and apply it to take appropriate action. The information that we receive through our eyes or sensory visual information is vast and complex [6]. This input from the outside world needs to be interpreted and processed in order for us to make any reasonable use of it.

Processing visual information is demanding and intricate. Therefore, a large part of humans' cortex is related to that function [2]. Hierarchy of different visual areas are occupied with that task. They communicate back and forth to interpret the information from sensory input [6]. A lot of decisions and predictions are made about the world to end up with an image we consciously perceive and interpret [2]. The human mind seems to do it so effortlessly that we hardly ever think about how complicated this process can be.

The fact, that the human brain is incredible at performing visual tasks that it is presented with every day, becomes even more evident when we present similar tasks to computers. The most successful attempts in object recognition from images has been made with deep learning [3]. As in the case of the brain, deep learning uses hierarchical method to recognize an object. It builds abstract features and complex objects from very simple features.

This thesis explores human brain activity during a visual recognition task. Data for this purpose were collected from patients with implanted intracranial electrodes. During the experiments the patients were shown images from various image categories while electrodes were recording brain's responses. The thesis concentrates on a certain type of neural activity, the so-called high-gamma

activity, which typically occurs in the frequency range 70-150 Hz. This particular frequency band reflects local neuronal activity and has been connected with such brain functions as attention and visual processing [16].

The aim of this thesis is to characterise how neural activity represents different classes of images. In particular, it is studied how various images elicit activity in the brain, more specifically the high-gamma activity, using different techniques of unsupervised machine learning to try to find clusters or structure within the dataset based on intracranial brain recordings.

The thesis consists of three main chapters. First of these (Methods) describes the origin of the dataset and the analysis methods used in this thesis. In the following chapter the results of the of visualizing images and electrodes as well as outcomes of biclustering are presented. Finally, the interpretation of the results of the data analysis is given. In addition, the limitations and future work connected to this thesis are discussed.

2 Methods

2.1 Collecting data

Dataset used in this thesis represents human brain activity during visual stimuli task. Information was collected in the University Hospital of Lyon from patients with drug-resistant epilepsy. Intracranial electrodes were used to monitor brain activity in order to locate the exact source of epileptic seizures of patients before performing surgery. Since using intracranial electrodes to monitor brain activity is considered to be an invasive method, it is only used when there is a clinical reason for implanting them. During the observation period in the hospital 109 individuals gave their consent to participate in an experiment (unrelated to epilepsy) involving a visual recognition task.

The detailed information about the task procedure is described in [16]. Pictures used in the experiments were divided into different groups. These image categories included animals, faces, fruits, houses, scrambled images, (nature) scenes and tools. Each of them were represented 50 times, except for fruits, which appeared 19 times. An image appeared every 1000-2000 ms and was

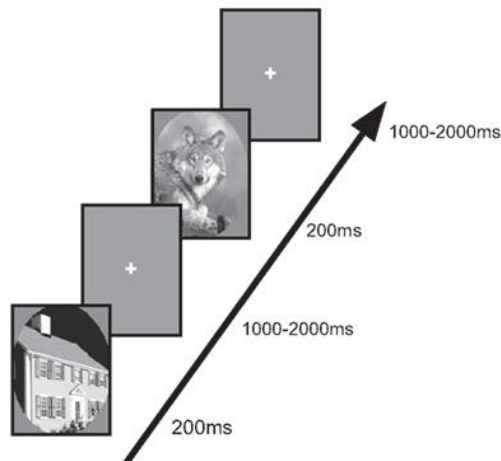


Figure 2-1. Protocol of stimulation. Images are shown every 1000-2000 ms for 200ms while the neural activity of the patients is recorded. Image taken from [16]

shown for 200 ms. Viewers could rest their eyes for 3 seconds after every fifth picture. The succession of presenting images is illustrated in Figure 2-1.

Throughout the experiments the intracranial electrodes recorded brain activity of the patients. The dataset analysed in this thesis consists of pre-processed data of that activity in the high-gamma band from electrodes positioned in the brain regions known to be involved in handling visual information.

In order to extract the high-gamma band activity from the brain recordings, the data were filtered using wavelet transform. This method enables to have certain frequency resolution without losing the temporal resolution altogether. Frequency range that was examined was 70-150 Hz [8, 12]. The entries in the data matrix correspond to the power in the investigated range at a window of 50-350 ms after an image was shown and divided by the analogous power 400-100 ms before the picture was presented to the patient. As a result, the values express the neural response to the image compared with the baseline activity before the image was shown.

Overall, the pre-processed data represent the activity elicited by 319 different images. Electrodes chosen for this theses were form brain regions which have been connected to the processing visual information. These are Brodmann areas 17, 18, 19, 20, 27, 28, 35, 37 and 38. The positions of these regions in the brain can be seen in Figure 2-2. After selecting these electrodes, we are left with 537 entities representing the electrodes. Therefore, the dataset is represented by 319 x 537

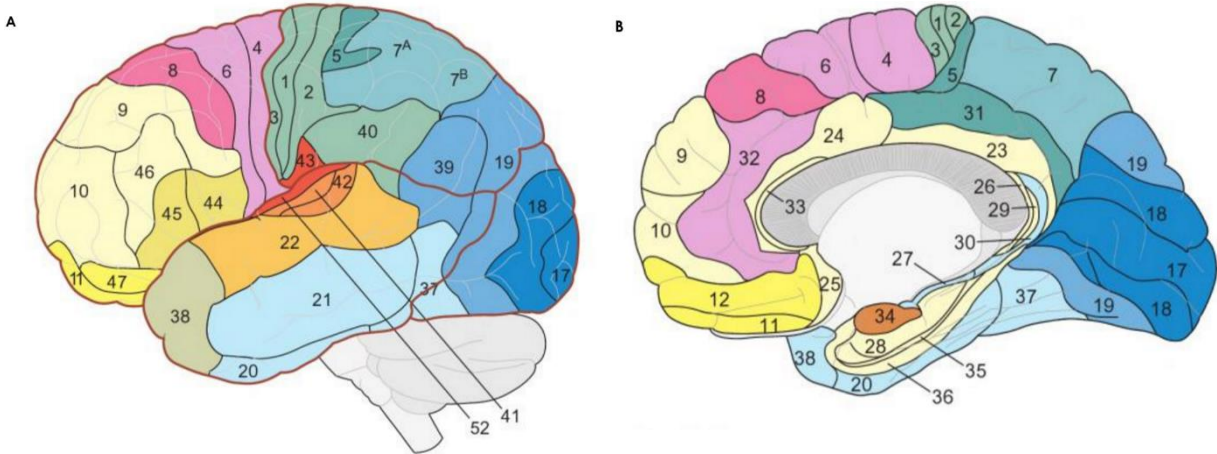


Figure 2-2 Brodmann areas in the brain. (A) Lateral view of the left hemisphere (B) Midsagittal view of the right hemisphere. Image taken from [2]

matrix with rows characterising pictures shown in the experiments and columns symbolising the different electrodes in the appropriate regions.

2.2 Analysing methods

The dataset of the high-gamma band responses to images was analysed with unsupervised machine learning techniques to discover structure in the data. These methods fall into the following general categories: visualization and biclustering. The programming language used to conduct this analysis was Python 2.7 and all of the implementations of machine learning algorithms came from scikit-learn library.

2.2.1 Visualization

Visual representation of data can be helpful for understanding the structure of information it contains. Visualization of high-dimensional data however, is challenging. The numerous features of a data point make it difficult to accurately visually describe data in low-dimensional space, which is more easily interpretable. In order to represent high-dimensional data in for example two dimensional Euclidean space, dimensionality reduction [15] is needed. There are number of algorithms devised to undertake this very issue while attempting to maintain as much of the original structure of the high-dimensional data as possible. One of these techniques is the t-Distributed Stochastic Neighbor Embedding method.

2.2.1.1 *T-Distributed Stochastic Neighbor Embedding*

The description of T-SNE or t-Distributed Stochastic Neighbor Embedding is based on the article of the developers of the method – Laurens van der Maaten and Geoffrey Hinton [14]. T-SNE is a visualization technique for high-dimensional data. The algorithm uses non-linear dimensionality reduction in order to map data points from higher dimensions to two or three dimensions so that similar objects are represented by nearby points.

Pairwise distances in high-dimensional space are transformed into symmetrized conditional probabilities that represent similarities. There are various metrics that can be used for measuring distances between data points. In this thesis Euclidean distance and cosine dissimilarity are used. The probabilities are calculated using Gaussian distribution centred on each data point. Perplexity (2 to the power of Shannon entropy) is taken as a parameter of the algorithm to determine the size of variance σ of the distribution.

Similar conditional probabilities are also calculated with data points in the lower dimension, but instead of the Gaussian distribution the Student-t distribution used since the latter has heavier tails. That means that points that are fairly dissimilar from each other in the high-dimensional space are pushed further apart in lower dimension, which helps to draw out different clusters. The final result of the algorithm comes from the minimisation of Kullback-Leibler divergence between these probabilities from high and low-dimensional space.

2.2.2 Biclustering

Clustering or cluster analysis [1] is a way of analysing data resulting in data points being organized into a number of clusters or collection of data points based on some criteria of similarity. The means of reaching this objective are diverse. It can vary in the strategy of forming the clusters or ways of defining a cluster. Therefore, there are many algorithms devised to tackle this task.

One of the most common of them is k-means clustering algorithm [9]. The aim of this method is to minimize the differences of objects belonging to one cluster. The algorithm assigns every data point to a centroid it is closest to. Points assigned to the same centroid form a cluster. The new mean of the cluster is calculated and it becomes the new centroid. This continues until there is no significant change.

Clustering is a useful tool for analysing data. Usually it is done by only clustering rows or columns of a data matrix (that is, separately). Biclustering [4, 10] however is clustering rows and columns at the same time to find significant submatrices formed of similar rows and columns. As in the case of clustering, there are many different algorithms diverse in their nature to resolve this analysis problem. In this thesis we used the Spectral Co-clustering method explained below.

2.2.2.1 Spectral Co-Clustering

Spectral Co-Clustering [10] tries to find subset of rows and columns that are significantly dissimilar from other rows and columns of the data matrix simultaneously. The output of the algorithm is the rearrangement of these subsets so that clusters are formed. Each column and each row of the data matrix belongs to exactly one of these clusters. When the outcome of Spectral Co-Clustering is visualised, it can be seen that the determined subsets or biclusters are arranged as blocks along the diagonal. Illustration how the algorithm recovers original structure from after the initial data were shuffled is shown in Figure 2-3.

The description of Spectral Co-clustering algorithm in this thesis is based on its detailed description in [5]. The method is so named because separating the most similar subsets of columns and rows is accomplished by spectral graph partitioning. The row and column indexes of the data matrix are interpreted as vertices of a graph. The value in column e in row i corresponds to the edge weight between vertices e and i . In order to divide the resulting bipartite graph so that vertex subsets are of equal size, the graph is partitioned with optimal normalized cut.

The optimal partitioning of the graph of original data matrix A to two subgraphs can be achieved by finding the second largest eigenvector of the Laplacian matrix of the graph. It is however computationally more efficient to calculate the equivalent second singular vectors of normalized matrix $A_n = D_1^{-1/2}AD_2^{-1/2}$ instead. D_1 and D_2 are degree matrices according to rows and columns of

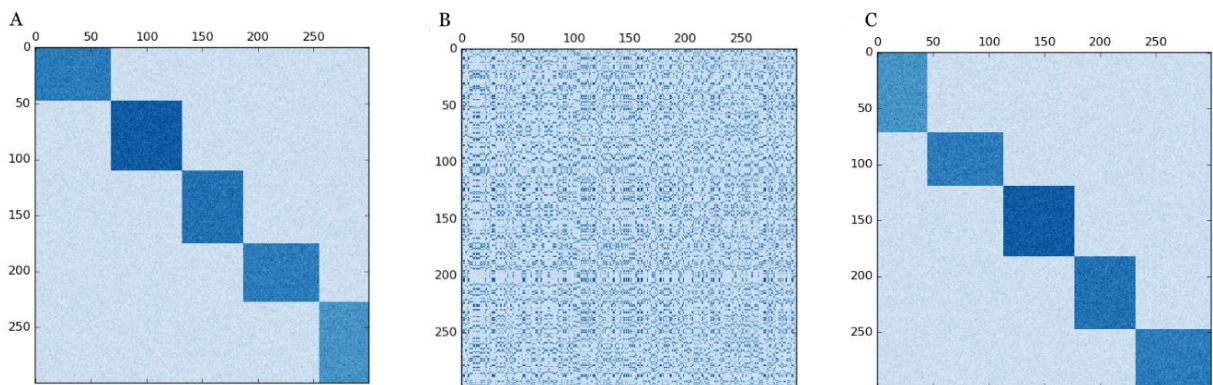


Figure 2-3 Results of Spectral Co-Clustering. (A) Original dataset with structure (B) Dataset after shuffling (C) Recovered structure after applying the algorithm [11]

the initial data matrix A . Based on the previous observation, the partitioning to find k biclusters can be accomplished by computing $l = \lceil \log_2 k \rceil$ smallest singular vectors starting from the second smallest. The final repositioning of rows and columns is determined by using k-means clustering algorithm.

3 Results

In this chapter, the results of analysis of the dataset with unsupervised machine learning algorithms is presented. The study of the structure of the high-gamma activity data is divided into three subsections to describe the visualization of image groups, visualisation of electrodes and finally the biclustering of the data matrix.

3.1 Structure across images

The 319 images in the dataset belong to seven different categories. Each of these has a number code, which is the following: houses (10), faces (20), animals (30), (nature) scenes (40), tools (50), fruits (80) and scrambled images (90). The goal of visualizing data points representing images to find characterizing clusters of responses is to find to what extent these groups form clusters according the reaction of the brain recoded by the electrodes in visual areas.

The results of applying t-SNE with Euclidean distance and perplexity set to 15 can be seen in Figure 3-1. There does not appear any distinguished clusters or collection of points that are clearly

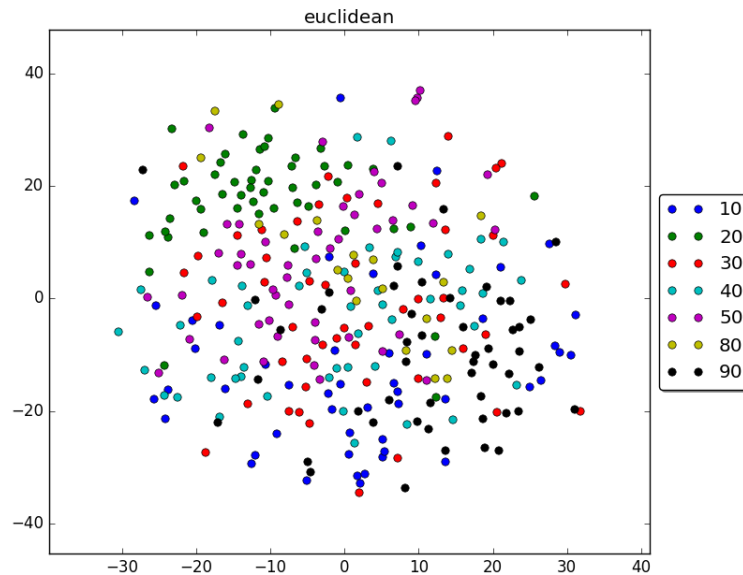


Figure 3-1 Visualization results of images with Euclidean distance

separated from other data points. All of the points in the figure form one big cluster. However, if we look at how different colours are dispersed in this cluster, some structure can be distinguished.

There appears to be a green cluster of data points in the top left corner of the image. This is the most homogenous group in this figure. Big proportion of the points marked 20 (they represent faces) are gathered to this area and there does not seem to be many points from other image groups in the midst of these.

The opposite side of the figure is largely populated by points from groups 10 and 90. The black data points (90) indicating scrambled images appear in the bottom right corner of the big cluster. They are not concentrated as well together as the pictures of faces are and there are other image groups spread in the gaps between them, but they are positioned relatively close together. The dark blue points (10) are mostly dispersed along bottom edge of the large cluster. These points representing houses are mostly scattered in the same region of the figure, but there here is no uniform cluster formed.

The area of the cluster between faces and houses and scrambled images is more varied in groups than the previously discussed. The pale blue points (40) signifying (nature) scenes are a little more populated closer to houses and scrambled pictures and magenta points (50) representing tools are

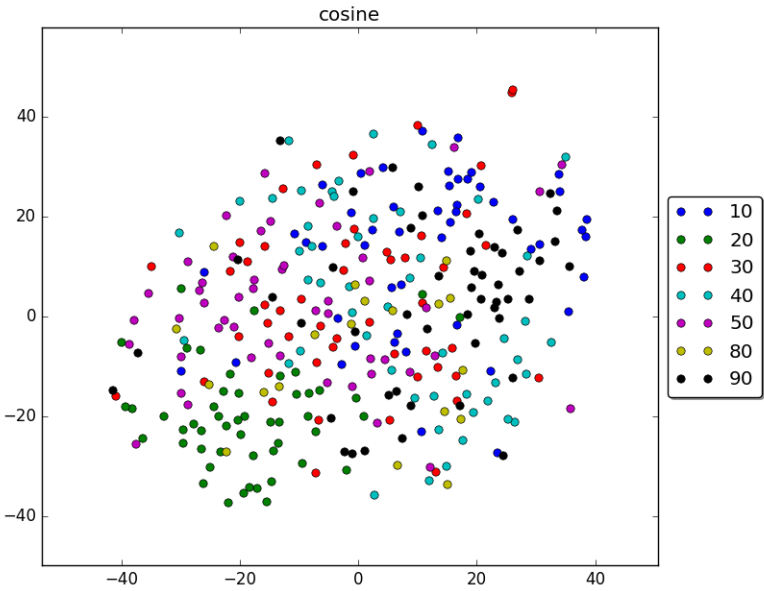


Figure 3-2 Visualization results of images with cosine distance

mostly adjacent to faces but there is no clear line of distinction or clustering between them and both image groups are rather widely dispersed. Yellow (80) and red (30) data points, signifying fruits and animals respectively, appear to be scattered in various parts of the figure and they do not form a cluster or occupy a visibly distinguishable area.

When t-SNE is applied to the dataset with the same parameters but with cosine dissimilarity as distance metric, the results are at first appearance similar to those with the Euclidean distance. Nonetheless, there are some differences in the outcomes. The results with cosine distance as the metric are shown in Figure 3-2.

As in the figure with Euclidean distance, there are no distinct clusters that are noticeably separated from other data points, but there are different areas which have higher concentration of some image groups and very few from other categories. The data points signifying faces (20) still form the most distinct cluster in the figure. Green points in the bottom left corner are for the most part close together and there appear very few odd data points from other image groups.

The houses that occupied the bottom area of the cluster in Figure 3-1 are more concentrated in Figure 3-2. The dark blue points (10) are mostly positioned on the top right corner of the image. There are data points from other image groups scattered among those representing houses, but there is noticeable improvement in the clustering of these points. A number of scattered images (90) form a visible cluster on the right from the houses. However, there are few scattered black spots that are separate from that collections of points.

The points representing the depictions of nature scenes (40) form two very faint groups. One of them is in the top part of the figure and is somewhat mixed with houses (10) and tools (50). The other is on the right edge of the figure and seems to be less disturbed by other image groups. Still there is no uniform cluster of light blue cluster emerging.

Same can be said about data points of tools (50) which are manly positioned in the centre of the big cluster above data points representing faces. They are rather broadly scattered and are largely mixed with points from other groups. As with the Euclidean distance, there is no structure emerging among points signifying fruits (80) or animals (30) since both image categories are widely dispersed in the figure.

Similar results were obtained when parameters of the t-SNE such as the perplexity and initial dimension were varied around the values used to report Figures. 3-1 and 3-2.

3.2 Structure of neural activity

In the dataset there are 537 electrodes selected from the recordings data. These electrodes were positioned in nine different Brodmann areas: 17, 18, 19, 20, 27, 28, 35, 37 and 38. These brain regions have been connected to processing visual information. The objective of visualizing electrodes is to find structure in the form of clusters or subsets of electrodes which recorded similar activity taking into account all images in the dataset. That is, to find which areas of the brain respond similarly when presented with images.

To visualize available high-dimensional data in two dimensional Euclidean space, the t-SNE algorithm is applied. Since the number of samples and their features is high in the dataset (537 x 319), principal component analysis is used as initialization of embedding in the case of visualizing electrodes to somewhat reduce the dimensionality of the data to speed up computation of the t-SNE algorithm.

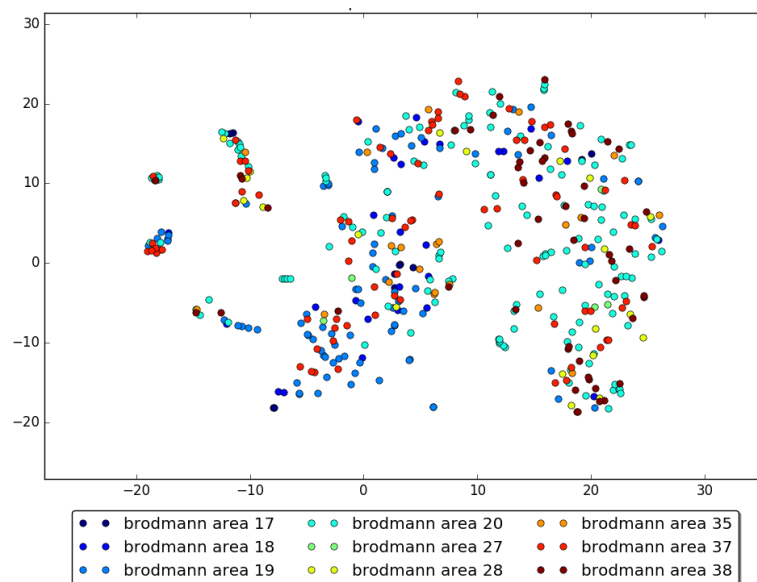


Figure 3-3 Visualization results of electrodes with Euclidean distance. Initialization of embedding = 10, perplexity = 15

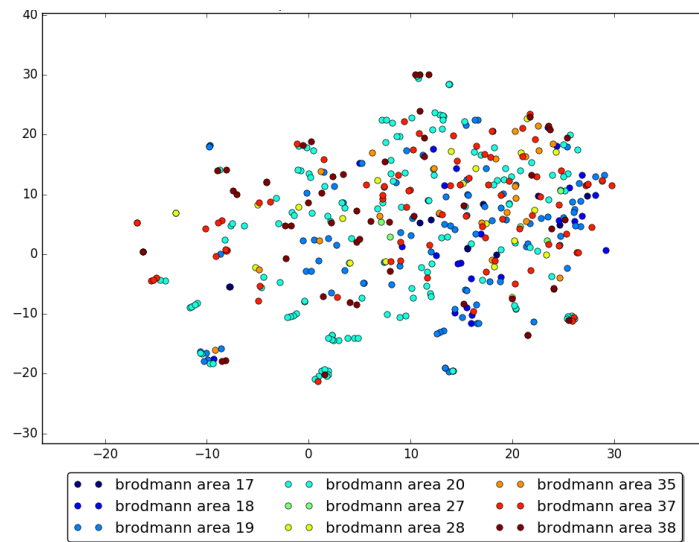


Figure 3-4 Visualization results of electrodes with normalized data and Euclidean distance. Initialization of embedding = 10, perplexity = 15

The results of t-SNE using Euclidean distance as a dissimilarity measure can be found in Figure 3-3. In the mentioned figure there are two clear larger clusters and on the left few smaller clusters. The groups are dispersed over several Brodmann areas. However, in the cluster in the centre of the figure, there is clear domination of data points from areas 18 and 19. This collection of points can be further divided into two smaller clusters, bottom of which has even a higher proportion of the previously brought up areas.

The biggest cluster in the figure consists of data points from all Brodmann areas in the dataset. It can be observed that the centre of this cluster mainly scattered data points from area 20 somewhat mixed with points from areas 38, 37, 35, 28 and 19. Top and bottom regions of this group are even more mixed with electrodes from other areas.

When the dataset is normalized according to electrodes (for each electrode the sum of its square values across all images is 1), the previous clusters collapse into one big cluster (shown in Figure 3-4). Although it is still visible that points from areas 17, 18 and 19 gather mostly to the right hand side of the figure. The data points from Brodmann area 20 are scattered predominantly on the left half of the cluster. It is notable that a small cluster of data points in the bottom left in Figure 3-3 survives normalization and can be seen on the left of the big cluster in Figure 3-4.

The smaller clusters from Figure 3-3 can also be observed when cosine similarity is used instead of Euclidean distance (see Figure 3-5). Similarly, with the previous notion of distance, there appear two larger clusters. The nature of these clusters is somewhat different from the ones in the previous

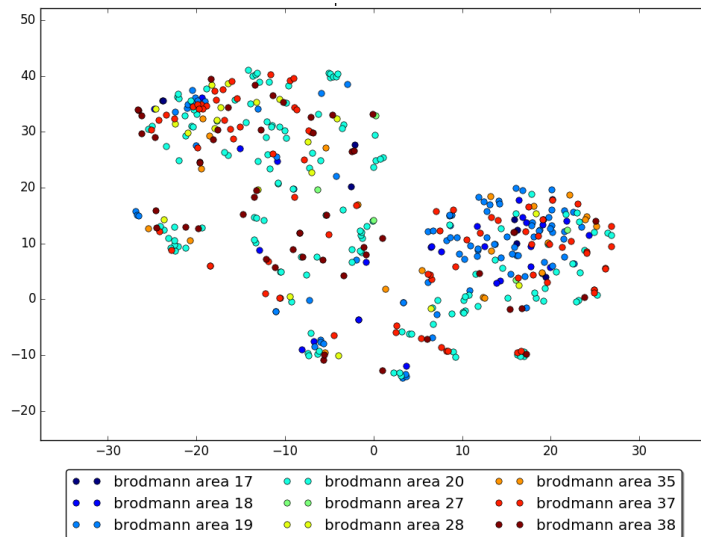


Figure 3-5 Visualization results of electrodes with cosine distance. Initialization of embedding = 10, perplexity = 17

figure. The concentration of data points from areas 18 and 19 is even more evident in the cluster on the right. The other larger cluster on the left in the figure can be parted into two different areas. Top left part of this group is denser and it contains one strongly connected collection of points which is similar to the small cluster that appears in the far left on the Figure 3-3. Data points in the centre of Figure 3-5 are more sparsely positioned and consists largely of points from Brodmann area 20.

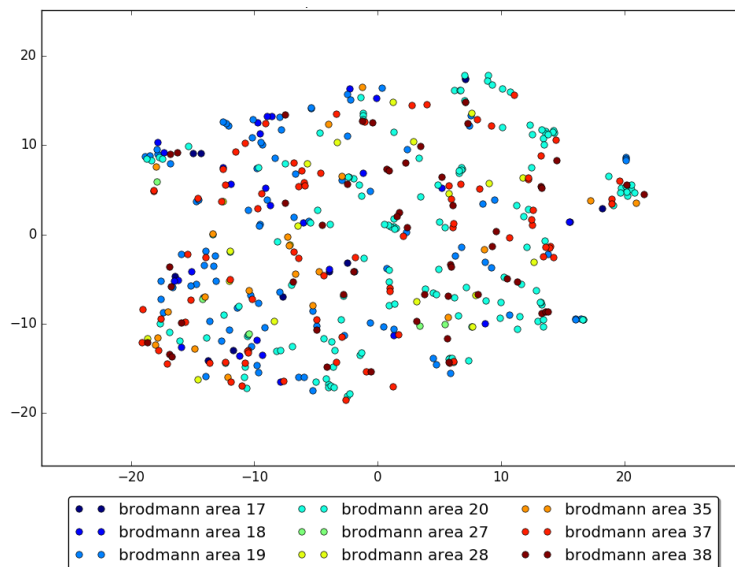


Figure 3-6 Visualization results of electrodes with normalized data and cosine distance. Initialization of embedding = 10, perplexity = 17

As in the case of Euclidean distance, when data are normalized, the clear clusters collapse as shown in Figure 3-6. Also the data points from Brodmann areas 17, 18, 19 appear mostly on the left side of the figure and more scattered points from area 20 appear on the opposite side of it. In the top left corner, there appears the small cluster that also can be seen on all three previous figures.

3.3 Biclustering

While the objective of clustering is to find similar entities across all rows or column, two-way clustering tries to pick out subsets of both to form submatrices that are called clusters or biclusters. The aim of biclustering in this instance is to find images that elicit similar neural activity recorded by a certain subset of electrodes.

Dataset containing the information about high-gamma activity consist of real values. The inherent variability of neural data makes the high-gamma activity represented by real numbers a very noisy signal in the context of biclustering. To make the data more manageable for the algorithm, the values in the matrix are given binary/ternary values according to certain thresholds. These thresholds were chosen based on the histogram of the entry values in the data matrix (the histogram can be seen in Figure 3-7).

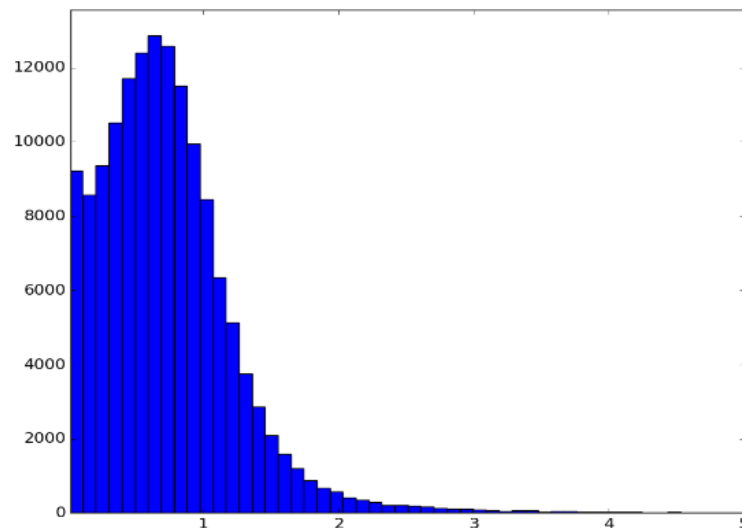


Figure 3-7 Histogram of the values of the data matrix

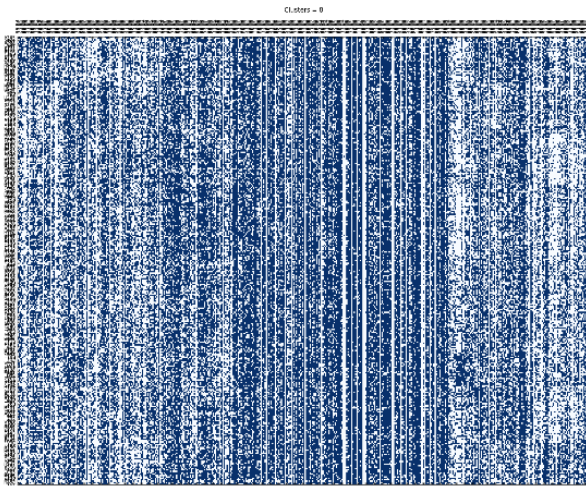


Figure 3-8 Result of Spectral Co-clustering with binary data

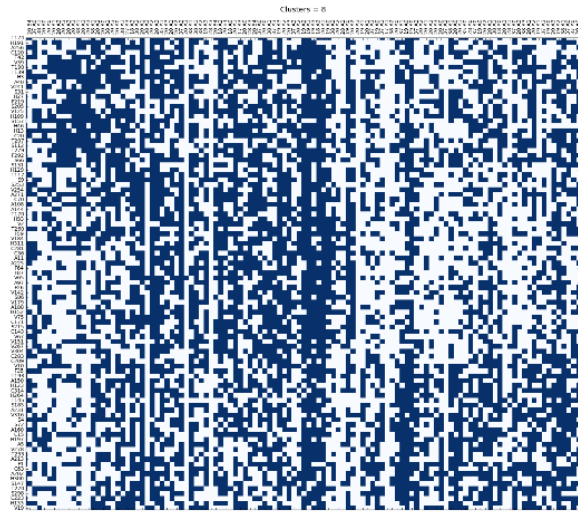


Figure 3-9 Bottom right clusters of Spectral Co-clustering with binary data

The binary threshold values considered for this dataset were 1 and 0.6. The value 1 has a special meaning in the context of this data. It signifies that the recorded activity during the time image presented was equal to the activity before the picture was shown (there was no change). The 0.6 was chosen as a representation of the highest peak on the histogram of dataset values. The values smaller than the threshold were given the value 0.1 and the value 1 was given to real values greater or equal to the threshold.

Ternary values selected for threshold pairs were the following: 0.5 and 2, 0.25 and 1.25. Low activity values under the lower threshold were given the value 0.1. Majority of values stayed in the interval between the thresholds and were given the value 0.5 while the highest real values were represented with the value 1.

Spectral Co-Clustering algorithm requires the number of the clusters to be determined before running the algorithm. Since there is no prior information about the amount of biclusters that the dataset at hand could contain, there was a large variety of bicluster numbers tried to find structure in the data.

Best results of co-clustering of binary data are obtained using the threshold 0.6 while the number of biclusters to find is set to 8. The result of the arrangement of rows and columns after the biclustering can be seen in Figure 3-8. There appear some unclear biclusters (rectangular patterns) but there are no strong patterns emerging. Closer look at the structure of examples of the mentioned clusters are presented in Figure 3-9. The large number of straight vertical lines in the

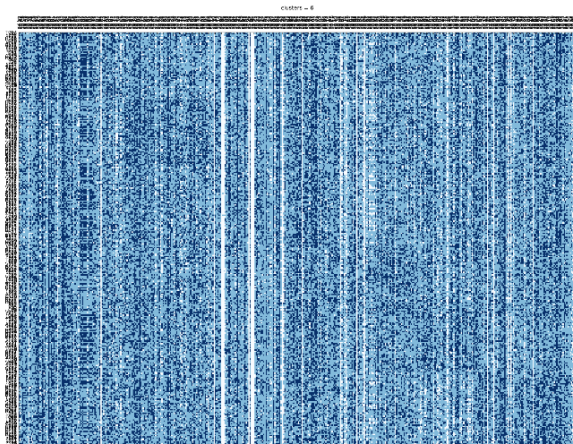


Figure 3-10 Results of Spectral Co-clustering ternary data

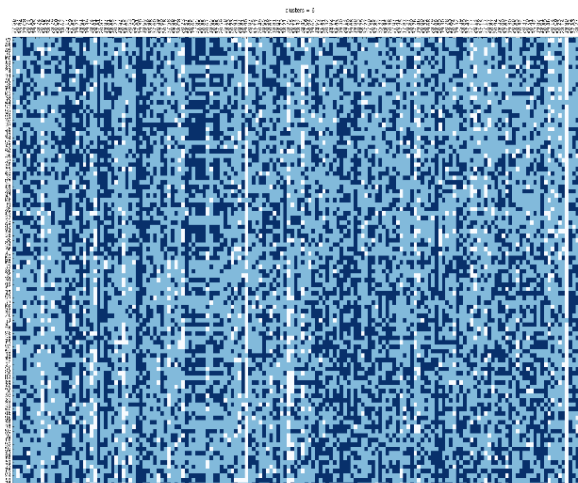


Figure 3-11 Bottom right clusters after applying Spectral Co-clustering on ternary data

figure show that many of electrodes pick up similar high-gamma activity when any of the images is presented.

The results with the matrix of ternary values that were acquired with applying the thresholds 0.25 and 1.25 were better than those with the threshold values 0.5 and 2. The biclusters in the figure were most noticeable when the number of clusters was set to 6. The outcome of Spectral Co-clustering algorithm with ternary data can be seen in Figure 3-10. As in the case of binary data it is possible to see some clusters appearing on the diagonal of the figure but the structure is not very clear. This is even more noticable when these biclusters are inspected more closely, as can be seen in Figure 3-11.

When studying the results of Spectral Co-clustering in Figure 3-8 and in Figure 3-10, it is apparent that even though matrices with binary and ternary values were used instead of the real value dataset, they are still relatively noisy. Even in the case of the most promising results, the outline of biclusters is faint.

The dataset was rearranged in order to find if the results of the co-clustering are significant. Each column of the matrix was shuffled independently to disorganize the data while preserving its global statistics (mean, etc.). As seen on Figure 3-12 and Figure 3-13, the co-clustering of the rearranged matrix with the same parameter values also gives weak clusters as a result, similar to the results of co-clustering the original dataset. Therefore, it is probable that the data do not contain meaningful biclusters that are discoverable with this method with the parameters that we scanned.

There are also no noteworthy results with the Spectral Biclustering [7, 10] method, which like the Spectral Co-Clustering algorithm uses eigenvalues to find clusters in the data, but instead of placing significant submatrices on the diagonal of the figure, it expects to find a checkerboard structure in the data.

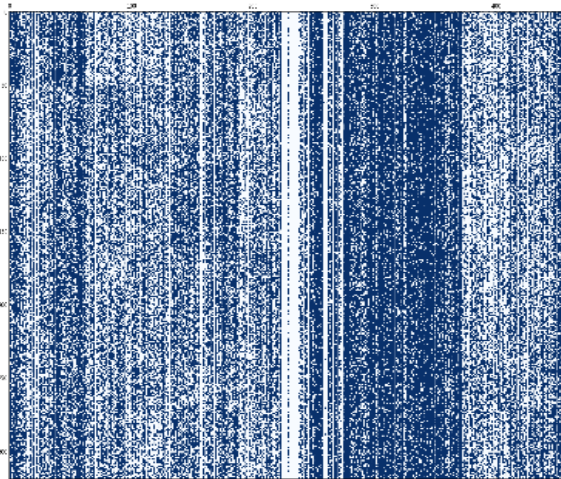


Figure 3-12 Spectral Co-clustering of scrambled binary data

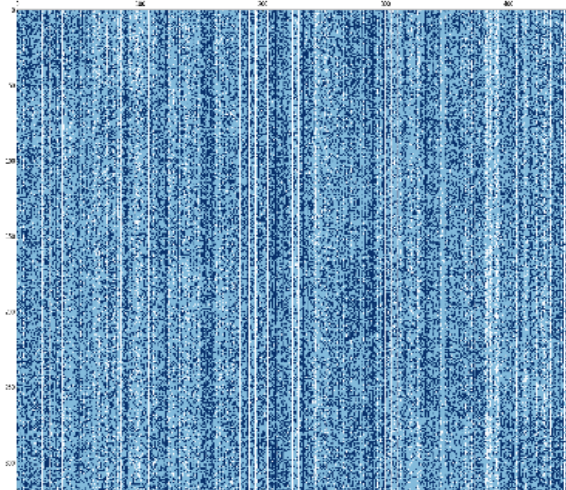


Figure 3-13 Spectral Co-clustering on scrambled ternary data

4 Discussion

4.1 Interpretation of results

The visualization of images with t-Distributed Stochastic Neighbor Embedding suggests that there is some structure appearing amongst high-gamma responses to pictures in the visual areas of the human brain. The faces are most distinctly clustered of the image categories with both Euclidean and cosine distance. The neural response to faces is very different from that of the houses and scrambled images. The latter two do not cluster as well as faces, but there is some noticeable structure, especially when cosine distance is used as a metric. This is in accord with previous studies [16] that suggest that high-level representations of important objects are represented in different regions of the brain. It is known that faces are very special kind of stimuli for human beings and hence our results fit with the prior research showing that there are special areas in the brain devoted to faces [13].

Visualizing electrodes from Brodmann areas 17, 18, 19, 20, 27, 28, 35, 37 and 38 resulted in the formation of clearly defined clusters, which however were largely not homogenous from the aspect of areas collected in them. With both metrics used (Euclidean and cosine distance) there appeared some small clusters and two large clusters. The latter differed according to the notion of distance used. When the data were normalized the clusters collapsed but some of the characteristics of the positioning of data points was still present. Such a collapse might represent that different sets of electrodes had a global higher response to all images than others sets of electrodes.

The biclustering with the method of Spectral Co-clustering gave no notable results with the dataset used in this thesis as there was no significant pattern found in the outcome after applying the algorithm, since the weak clusters formed were similarly present in the case scrambled data were used.

4.2 Limitations

Main limitations for this theses were the number and precision of the electrodes that recoded the human neural activity. Overall there were more than 12 000 electrodes recording the brain activity from 109 patients. The intracranial electrodes are only implanted in humans if there is a clinical purpose and necessity for it and they are only implanted in the areas where they are needed. Therefore, only 537 of these electrodes were in the Brodmann areas that were of interest in the context of this theses. That is, in the brain regions that have been connected with processing visual information. While this is a very large number of electrodes for the type of studies they were collected, it still represents a very small fraction of the tissue in the visual cortices. Also, since the data is taken from a number of patients the particularities of the brains of different patients also needs to be taken into account.

4.3 Future work

The future work in analysing high-gamma activity elicited by images could include more methods of biclustering data since there is only one of these methods thoroughly studied in this thesis out of many diverse algorithms. It would be interesting to examine these techniques with various notions of distances. Distance learning algorithms are also an interesting possibility to find the notion of distance that best separates the different classes (images or Brodmann areas) of the data.

Future studies could also explore studying neural activity during visual task in frequency bands other than high-gamma with unsupervised machine learning method. As well as comparing the results of these analysis with different frequencies.

As for using the outcomes of this thesis for future work, the results of visualizing electrodes in different Brodmann areas with t-SNE found in section 3.2. of this thesis could be further studied on a 3D model of a brain to obtain additional information about the clusters formed.

5 Conclusion

The objective of this thesis was to examine high-gamma activity in the human brain elicited by visual stimuli in the form of pictures from different image categories. This was done with techniques of unsupervised machine learning, more specifically visualization (with the t-SNE algorithm) and biclustering (with Spectral Co-clustering).

The latter did not provide any significant outcomes. Visualization results however brought out some structure in the data. In the case of images, patterns relating to image groups such as faces emerged. Applying t-SNE showed electrodes forming distinct clusters containing data points from numerous Brodmann areas.

6 References

- [1] C. C. Aggarwal, *Data mining: The textbook*: Springer, 2015.
- [2] B. J. Baars and N. M. Gage, *Cognition, Brain, and Consciousness: Introduction to Cognitive Neuroscience*: Academic Press, 2007.
- [3] Y. Bengio, I. J. Goodfellow, and A. Courville, "Deep learning," *An MIT Press book in preparation*. Draft chapters available at <http://www.iro.umontreal.ca/~bengioy/dlbook>, 2016.
- [4] M. Charrad and M. B. Ahmed, "Simultaneous clustering: A survey," in *Pattern Recognition and Machine Intelligence*, ed: Springer, 2011, pp. 370-375.
- [5] I. S. Dhillon, "Co-clustering documents and words using bipartite spectral graph partitioning," in *Proceedings of the seventh ACM SIGKDD international conference on Knowledge discovery and data mining*, 2001, pp. 269-274.
- [6] J. J. DiCarlo, D. Zoccolan, and N. C. Rust, "How does the brain solve visual object recognition?," *Neuron*, vol. 73, pp. 415-434, 2012.
- [7] Y. Kluger, R. Basri, J. T. Chang, and M. Gerstein, "Spectral biclustering of microarray data: coclustering genes and conditions," *Genome research*, vol. 13, pp. 703-716, 2003.
- [8] K. J. Miller, E. C. Leuthardt, G. Schalk, R. P. Rao, N. R. Anderson, D. W. Moran, *et al*, "Spectral changes in cortical surface potentials during motor movement," *The Journal of neuroscience*, vol. 27, pp. 2424-2432, 2007.
- [9] P. Rai and S. Singh, "A survey of clustering techniques," *International Journal of Computer Applications*, vol. 7, pp. 1-5, 2010.
- [10] Scikit-learn.org. (2016, 5. May). 2.4. *Biclustering*. Available: <http://scikit-learn.org/stable/modules/biclustering.html>
- [11] Scikit-learn.org. (2016, 5. May). *A demo of the Spectral Co-Clustering algorithm*. Available: http://scikit-learn.org/stable/auto_examples/biclust/plot_spectral_coclustering.html
- [12] M. M. Smith, K. E. Weaver, T. J. Grabowski, R. P. Rao, and F. Darvas, "Non-invasive detection of high gamma band activity during motor imagery," *Frontiers in human neuroscience*, vol. 8, 2014.
- [13] D. Y. Tsao, W. A. Freiwald, R. B. Tootell, and M. S. Livingstone, "A cortical region consisting entirely of face-selective cells," *Science*, vol. 311, pp. 670-674, 2006.

- [14] L. Van der Maaten and G. Hinton, "Visualizing data using t-SNE," *Journal of Machine Learning Research*, vol. 9, p. 85, 2008.
- [15] P. E. van der MLJP and J. van den HH, "Dimensionality reduction: A comparative review," Tilburg, Netherlands: Tilburg Centre for Creative Computing, Tilburg University, Technical Report: 2009-0052009.
- [16] J. R. Vidal, T. Ossandón, K. Jerbi, S. S. Dalal, L. Minotti, P. Ryvlin, *et al.*, "Category-specific visual responses: an intracranial study comparing gamma, beta, alpha, and ERP response selectivity," *Frontiers in human neuroscience*, vol. 4, p. 195, 2010.

7 Appendix

Code used for the analysis can be found in:

<https://github.com/kpokk/Neural-Response-to-Images>

8 Licence

Non-exclusive licence to reproduce thesis

I, Kristiina Pokk

1. herewith grant the University of Tartu a free permit (non-exclusive licence) to:
 - 1.1. reproduce, for the purpose of preservation and making available to the public, including for addition to the DSpace digital archives until expiry of the term of validity of the copyright, and
 - 1.2. make available to the public via the web environment of the University of Tartu, including via the DSpace digital archives until expiry of the term of validity of the copyright,

“Exploring how images are represented in human brain activity”, supervised by Raul Vicente and Jaan Aru,
2. I am aware of the fact that the author retains these rights.
3. I certify that granting the non-exclusive licence does not infringe the intellectual property rights or rights arising from the Personal Data Protection Act.

Tartu, 12.05.2016